

## A mathematical model for brain tumor response to radiation therapy

R. Rockne · E. C. Alvord Jr. · J. K. Rockhill ·  
K. R. Swanson

Received: 12 June 2007 / Revised: 8 February 2008  
© Springer-Verlag 2008

**Abstract** Gliomas are highly invasive primary brain tumors, accounting for nearly 50% of all brain tumors (Alvord and Shaw in *The pathology of the aging human nervous system*. Lea & Febiger, Philadelphia, pp 210–281, 1991). Their aggressive growth leads to short life expectancies, as well as a fairly algorithmic approach to treatment: diagnostic magnetic resonance image (MRI) followed by biopsy or surgical resection with accompanying second MRI, external beam radiation therapy concurrent with and followed by chemotherapy, with MRIs conducted at various times during treatment as prescribed by the physician. Swanson et al. (Harpold et al. in *J Neuropathol Exp Neurol* 66:1–9, 2007) have shown that the defining and essential characteristics of gliomas in terms of net rates of proliferation ( $\rho$ ) and invasion ( $D$ ) can be determined from serial MRIs of individual patients. We present an extension to Swanson's reaction-diffusion model to include the effects of radiation therapy using the classic linear-quadratic radiobiological model (Hall in *Radiobiology for the radiologist*. Lippincott, Philadelphia, pp 478–480, 1994) for radiation efficacy, along with an investigation of response to various therapy schedules and dose distributions on a virtual tumor (Swanson et al. in *AACR annual meeting*, Los Angeles, 2007).

**Keywords** Modeling · Radiation therapy · Glioma · Linear-quadratic · Tumor response · Treatment fractionation

**Mathematics Subject Classification (2000)** 92B05

---

R. Rockne · E. C. Alvord Jr. · J. K. Rockhill · K. R. Swanson (✉)  
Department of Pathology, University of Washington, Washington, USA  
e-mail: swanson@amath.washington.edu

## 1 Introduction

Gliomas are highly invasive brain tumors that spread diffusely through the brain, producing life expectancies from 6 to 12 months [1, 5] for the most aggressive grade of gliomas known as glioblastoma multiforme (GBM). In practice, an algorithmic approach to glioma treatment includes a diagnostic magnetic resonance image (MRI) [6] followed by biopsy or surgical resection of varying extent and accompanying second MRI, external beam radiation therapy (XRT) concurrent with and followed by chemotherapy, with MRIs conducted at various times during treatment as prescribed by the physician.

Radiation therapy is used as a treatment for gliomas because of the precision with which it targets the tumor region, and its ability to increase survival as much as two fold [7, 8]. Assessing response to therapy in gliomas has historically focused on visible changes in gross tumor volume (GTV) as measured on MRI. Using the classic linear-quadratic model [3] for radiation efficacy, we extend Swanson's existing glioma model to include delivery and effect of radiation therapy. The advantage of a mathematical model in this case lies in the ability to observe tumor response at any point during therapy, and to virtually alter the treatment schedule and dose delivery, options not otherwise available *in vivo*.

We present Swanson's reaction-diffusion model [2, 9–11] which describes the diffusion and proliferation of tumor cells in addition to the effects of precisely delivered radiation therapy. Our model, although deterministic, is derived from stochastic first principles [32]. The diffuse nature of cell motility has an implicit basis in stochastics, since we can regard the random motion and migration of cells as Brownian motion, which gives rise to the diffusion equation [12]. Additionally, radiation therapy is an inherently stochastic process since its essential mechanisms are on the atomic level: particle collision, cell death, injury and random repair can all be seen as stochastic processes, and are essential to the derivation of the linear-quadratic radiobiological model, [3, 13–17] and therefore to the quantification of radiation therapy efficacy. Equally important is the deterministic modeling of the inherently stochastic spatial distribution of administered radiation dose in the tumor region.

Using *in vivo* radiation dose distributions as reference, we investigate the spatio-temporal delivery of radiation dose, treatment response, sensitivity and recovery time for various dose distributions and treatment fractionation schemes on a virtual tumor.

## 2 Model

### 2.1 Swanson's glioma model

Let  $c = c(x, t)$  represent the concentration of tumor cells per  $\text{mm}^3$  at a location  $x$  at time  $t$  where the domain  $\mathbf{B}$  (brain) is closed and bounded. What we will call Swanson's fundamental model is a reaction-diffusion partial differential equation which describes both the net diffusion and proliferation of tumor cells as follows:

$$\begin{array}{l}
 \text{rate of change} \\
 \text{of glioma cell} \\
 \text{concentration} \\
 \underbrace{\frac{\partial c}{\partial t}} \\
 x \in B, \quad t \geq 0, \quad c(x, 0) = c_0, \quad \mathbf{n} \cdot \nabla c = 0 \text{ on } \partial B
 \end{array}
 =
 \begin{array}{l}
 \text{net dispersal} \\
 \text{of glioma cells} \\
 \underbrace{\nabla \cdot (D(x)\nabla c)} \\
 +
 \end{array}
 +
 \begin{array}{l}
 \text{net proliferation} \\
 \text{of glioma cells} \\
 \underbrace{\rho c}
 \end{array}
 \quad (1)$$

where  $D$  is the spatially resolved diffusion coefficient [18, 19] with units  $\text{mm}^2/\text{year}$ ,  $\rho$  is the net rate of proliferation per year,  $c_0$  is the initial distribution of tumor cells, and a zero flux boundary condition  $\mathbf{n} \cdot \nabla c = 0$  which prevents cells from leaving the brain domain,  $\mathbf{B}$ , at its boundary  $\partial\mathbf{B}$ . Although Swanson’s model allows the diffusion coefficient to be a tensor to account for the complex geometry and preferential directions for cell migration in the brain [2], we consider here a one-dimensional, spherically symmetric and isotropic tissue environment where the diffusion is held constant at  $D$ .

An essential characteristic of this model is the formation of a tumor cell wavefront [20] which, in 3 dimensional spherical symmetry, asymptotically approaches a constant velocity,  $v = \sqrt{2D\rho}$ , Fisher’s approximation [12]. Although  $c$  could represent any tumor population, this simple reaction-diffusion equation is an appropriate model for gliomas in particular for several reasons:

1. Unlike tumors in other regions of the body, the highly diffuse nature and recurrence patterns [21] of gliomas agrees with essential properties of the model. Specifically, in as few as 7 days after tumor induction in a rat brain, glioma cells can be identified throughout the central nervous system [18], analogous to the instantaneous non-zero solution of the diffusion equation on any finite domain [22]. Additionally, recurrence of glioma growth at the boundary of resection mirrors the perpetual proliferation and dispersal of any non-zero tumor cell concentration at any time point [23].
2. In vivo evidence suggests the observably advancing tumor front travels radially at approximately a constant rate [24–27], and, barring treatment or physical barriers of brain anatomy, grows with spherical symmetry, aligning with Fisher’s approximation [2]. Moreover, the constant velocity of untreated growth suggests that  $D$  and  $\rho$  are characteristics intrinsic to the tumor [6, 28, 29].
3. The parameters  $D$  and  $\rho$  can be calculated for an individual tumor from as few as two pre-treatment MRI’s [2], eliminating the estimation and exploration of large parameter domains, and providing an immediately applicable metric for glioma growth and invasion for any given tumor in vivo.

### 2.2 Parameter ranges and estimation

Parameters  $D$  and  $\rho$  from Swanson’s fundamental glioma model can be computed from as few as two pre-treatment MRI observations [2, 6]. Current data from 29 tumors show a range of 6–324  $\text{mm}^2/\text{year}$  for  $D$  and 1–32 /year for  $\rho$  [2].

Despite the clinical relevance of Swanson’s fundamental model, it is only sufficient in describing untreated glioma growth. An extension of the model to include the effects

of resection and chemotherapy has been investigated [9–11,30]. However, in light of the pervasiveness of radiation therapy as a treatment to these tumors, an extension of the model to include the effects of such therapy is a natural and logical progression.

### 2.3 Extension to include radiation therapy

We introduce an extension to Swanson’s model of the form

$$\underbrace{\frac{\partial c}{\partial t}}_{\text{rate of change of glioma cell concentration}} = \underbrace{\nabla \cdot (D(x)\nabla c)}_{\text{net dispersal of glioma cells}} + \underbrace{\rho c}_{\text{net proliferation of glioma cells}} - \underbrace{R(x, t)c}_{\text{loss due to therapy}}, \tag{2}$$

where  $R(x, t)$  represents the effect of XRT at location  $x$  and time  $t$  [4]. We utilize the widely known and accepted linear-quadratic radiobiological model [3,31,32] for this extension, the motivation for which lies in our ability to communicate our modeling in a language familiar to our colleagues and collaborators in the medical community, as well as our belief in the relevance, versatility and robustness of the model.

Although XRT may be delivered in a variety of ways, the fundamental mechanism for cell death is linear energy transfer, or LET [31,32]. Highly energized particles are emitted from a radioactive source that ionizes the atoms which make up the DNA, causing lesions which can be thought of as injuries to the cell’s DNA. Cellular damage is manifested as double strand breaks (DSB) to the DNA structure. The DNA injury makes the cell unable to reproduce itself during the next mitotic phase since transcription will be impossible.

Since LET relies on a collision between an energized radiation particle and the DNA strand of a cell, there is an inherent stochasticity in measuring the effect of radiation, which we presume to be cell death. This manifests itself as a Poisson statistic [14] and provides the basis for the classic linear-quadratic (L-Q) model for radiation efficacy. The L-Q model can be derived in several ways, potentially utilizing disparate assumptions about cellular response, repopulation of cells and duration of dose delivery [13,33]. Although all have been shown to be equivalent, we prefer the derivation presented by Sachs et al [14], who showed that for a clonogenic cell population  $N$  the surviving fraction  $N/N_0$  can be expressed as a sum of linear and quadratic contributions to the log of the surviving fraction as

$$\ln \left( \frac{N}{N_0} \right) = -\alpha \tilde{D} - \beta \tilde{D}^2 \tag{3}$$

where  $\tilde{D}$  is the total dose administered,  $N_0$  and  $N$  are cell populations before and after therapy, respectively, and  $\alpha$  and  $\beta$  are parameters to be measured. This allows us to express the surviving fraction  $S$  of cells post radiotherapy as

$$S = \exp \left( -\alpha \tilde{D} - \beta \tilde{D}^2 \right). \tag{4}$$

In addition, it can be shown that cell population susceptibility based on increased radio-sensitivity in the G2 and mitosis phases of the cell cycle can be incorporated into the model derivation without formal change. Therefore our implementation of the L-Q model need not explicitly account for cell cycle dynamics, although that is a possible avenue for further investigation.

The L-Q model by definition relates the physical dose in units of Gray (Gy) which is the absorption of one joule (J) of radiation energy by one kilogram (kg) of matter,  $1\text{Gy} = \frac{\text{J}}{\text{kg}}$  to an effective dose (unitless) by the following relationship:

$$\text{effective dose} = \alpha \tilde{D} + \beta \tilde{D}^2. \tag{5}$$

In order to avoid toxic effects to normal tissue, the total dose is given in small fractions: where  $n$  is the number of fractions, and  $d$  is the fractionated dose which is implicitly spatially and temporally defined, so  $d = d(x, t)$  throughout. In practice, the ratio  $\alpha/\beta$  is held constant at 10 Gy [3, 14, 16, 34–37], and motivates the definition of the following quantities, derived from the *effective dose*(5) :

$$\text{BED} = nd \left( 1 + \frac{d}{\alpha/\beta} \right), \quad \text{relative effectiveness} = \left( 1 + \frac{d}{\alpha/\beta} \right) \tag{6}$$

where BED stands for the biologically effective dose, and is a convenient measure of efficacy: total dose times its relative effectiveness [3]. The definition of BED also leads to the following convenient expression of survival probability,

$$S(\alpha, d(x, t)) = e^{-\alpha \text{BED}}. \tag{7}$$

With  $\alpha/\beta$  fixed, and  $n$  and  $d$  determined by the treatment schedule, the strong dependence on the single parameter  $\alpha$  ( $\text{Gy}^{-1}$ ) is made clear. Large  $\alpha$  implies high susceptibility to therapy, whereas small  $\alpha$  implies low susceptibility: we therefore regard  $\alpha$  as our radiation sensitivity parameter.

It should be stated that several of the well known variations on the L-Q model [13, 16, 38] including cellular repopulation or loss rate and effective doubling time, are included in the net growth rate  $\rho$  in Swanson’s model (1).

Now that we have established the survival probability,  $S$ , as a function of the radiation sensitivity parameter  $\alpha$  and the dose distribution  $d = d(x, t)$  per fraction,  $(1 - S)$  represents the probability of cell death, and we can incorporate the effects of any radiation treatment protocol into Swanson’s fundamental model as follows:

$$\frac{\partial c}{\partial t} = \nabla \cdot (D(x)\nabla c) + \rho c - R(\alpha, d(x, t), t) c \tag{8}$$

where

$$R(\alpha, d(x, t)) = \begin{cases} 0, & \text{for } t \notin \text{therapy} \\ 1 - S(\alpha, d(x, t)), & \text{for } t \in \text{therapy}. \end{cases}$$

with space and time domains, as well as boundary and initial conditions as stated in (1).

### 3 Methods

#### 3.1 Model assumptions

For the purposes of initial exploration of the extended model, the following assumptions are made: in addition to the central assumption of isotropic spherical symmetry  $D(x) = D$ , our model assumes no effect of central or peripheral necrosis (cell death not already included in the net proliferation rate  $\rho$ ) on available space in the domain for growing tumor cells, or the direct induction or deceleration of cell diffusion or proliferation due to XRT. All effects of radiation on tumor cell concentration are instantaneous and deterministic, all cells are equally susceptible and likely to be killed by radiation as prescribed by the cell kill  $(1 - S)$  (7), and no delayed or otherwise toxic effects of radiation are considered.

#### 3.2 Non-dimensionalization and numerical algorithm

The model (8) is non-dimensionalized in one-dimension for computational convenience in the following way: introduce the non-dimensional quantities  $\bar{x} = x/L$ ,  $\bar{t} = \rho t$ ,  $\bar{c} = (cL^3)/c_0$  where  $L$  is the dimensional length of the computational domain, and  $c_0$  represents the initial number of tumor cells, which has no net effect on the scaling and is therefore arbitrary. This yields the following

$$\begin{aligned} \bar{c}_t &= D^* \nabla^2 \bar{c} - R^* (\alpha, d(\bar{x}, \bar{t}), \bar{t}) \bar{c} \\ \text{where, } R^* (\alpha, d(\bar{x}, \bar{t}), \bar{t}) &\equiv \begin{cases} 1, & \text{for } \bar{t} \notin \text{therapy} \\ \zeta(\alpha, d(\bar{x}, \bar{t}), \bar{t}), & \text{for } \bar{t} \in \text{therapy.} \end{cases} \end{aligned} \quad (9)$$

$D^* = D/(\rho L^2)$  and  $\zeta(\alpha, d(\bar{x}, \bar{t}), \bar{t}) = (1 - S(\alpha, d(\bar{x}, \bar{t}))) / \rho$  with scaled domains, initial and boundary conditions as previously stated and as in (1). All dimensional units are in the context of mm and years.

Model solutions are obtained using the one-dimensional discretization method of Skeel and Berzins [39] implemented in MATLAB. The algorithm utilizes a variation on a finite-element method which is second order accurate in both space and time, resulting in spatial resolution comparable with the most highly resolved MRIs, at 1 mm<sup>3</sup>. Clearly then, our measurement of tumor growth and response to therapy depend on the resolution of our spatial mesh, which need be no larger than what is measurable on MRI, therefore we take  $L = 200$  mm,  $\Delta x = 10^{-3}$  mm, and  $\Delta t = 1$  day. Moreover, we take  $n = 1$  in the formulation of the BED in order to consider the dose delivery and effect as a single, instantaneous event.

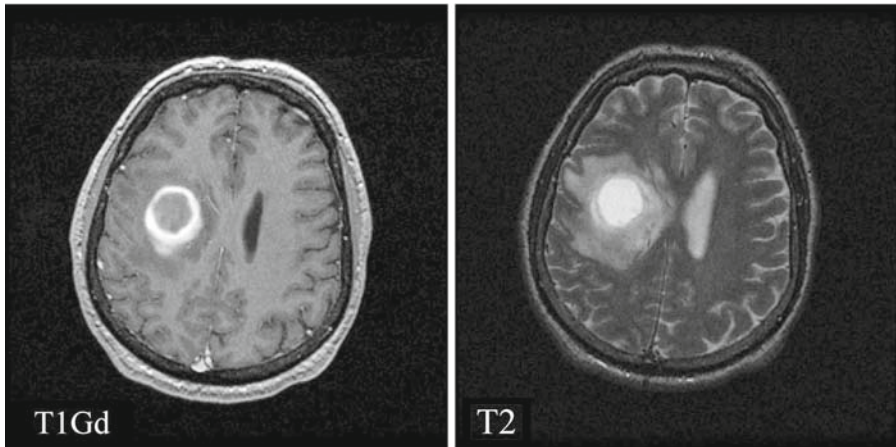


**Fig. 1** T1Gd and T2-weighted MRI images of a patient diagnosed with glioblastoma multiforme (GBM)

### 3.3 Initial condition

The extended, non-dimensional model (9) assumes an initial tumor concentration normally distributed as follows:

$$\bar{c}(\bar{x}, 0) = L^3 e^{-100\bar{x}^2} \quad (10)$$

where  $L$  is the length of the dimensional computational domain. The virtual tumor is allowed to grow until it reaches a specific size, corresponding to a radius between 10–20 mm, at which point radiation therapy is simulated. After the simulated therapy is completed, the tumor continues to grow for 100 additional days, at which point the simulation is completed.

### 3.4 MRI thresholds of detection

Clinical observation of glioma growth and progression relies primarily on MRI [6]. Swanson's model and analysis currently utilize gadolinium enhanced T1-weighted (T1Gd) and T2-weighted MRI imaging modalities. T1Gd images abnormally leaky vasculature within the tumor, outlining the bulk of the lesion. T2-weighted MRI captures edema as well as isolated tumor cells at a much lower threshold. Roughly speaking, the T1Gd MRI reveals the tumor mass, and the T2 the tumor's spread and associated swelling (edema), or clinically observable boundary (Fig. 1). Although the T1Gd abnormality outlines the neovasculature, and is thought to represent the bulk tumor mass, it is also potentially a poor indicator of response, as XRT damage may not cause rapid shrinkage of the abnormality. All clinical imaging modalities are limited by thresholds of detection, though it is well known that glioma cells infiltrate throughout the central nervous system well beyond any imaging abnormality [8]. Swanson's

model is able to act as an idealized imaging technique, allowing visualization of glioma cell concentration beyond what is visible on MRI.

### 3.5 Radiation dose delivery and distribution

Although our model allows for any imaginable treatment schedule or dose distribution, we define the standard treatment to be the current University of Washington Medical Center radiation protocol: 7 weeks of treatment, using a 5 days on, 2 days off schedule (to allow for weekends) delivering 1.8 Gy to the T2 enhancing region plus a 25 mm margin for 28 days, followed by 1.8 Gy to the T1Gd enhancing tumor region plus a 20 mm margin for the remaining 6 days, yielding 61.2 Gy total max dose to the tumor bed. The region and duration of the final 6 days is considered the boost time (BT) and boost region (BR), respectively. For simplicity, all treatment simulations are assumed to begin on a Monday so that 5 consecutive days of therapy can be applied before the 2 day rest period is implemented. The addition of the BT and BR make our dose distribution a function of time as well as space, so that  $d = d(x, t)$ .

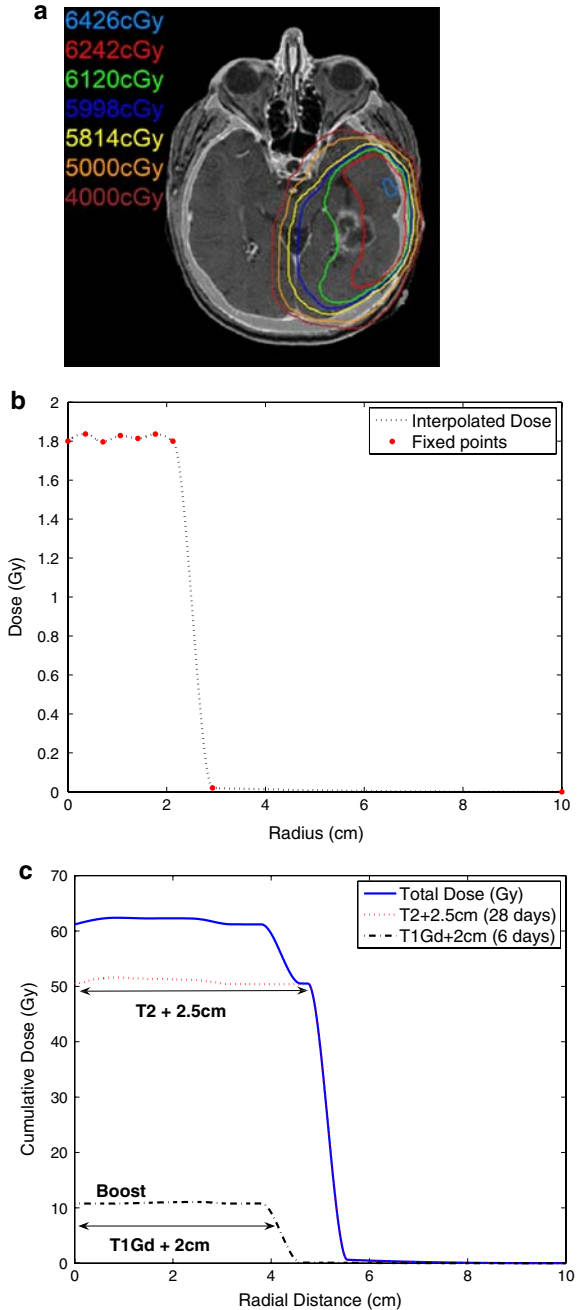
Days in therapy (DIT) is defined to be the duration of the therapy regimen, whereas days of treatment (DOT) is defined to be the number of days in which XRT was actually administered. For example, DIT = 35 days implies DOT = 25. In the case where DIT is not divisible by 7, the DOT is rounded to the next integer [40]. We consider DIT as individual, independent and instantaneous events each occurring on the day of treatment. In reality, treatment lasts several minutes each day. This assumption is consistent with the many derivations of the L-Q model, and poses no unnecessary or extraordinary abstraction from the mechanisms modeled.

In clinical practice, radiation dose is designed and delivered in a full 3-dimensional environment. Using 2-dimensional cross-sections of actual 3-dimensional dose distribution maps, with additional guidance from radiation oncologist Jason Rockhill, one-dimensional dose distributions were created for use in simulations using nine fixed reference points (Fig. 2) as follows: the target dose is fixed at the tumor center, with five points of random variation not to exceed 5% of the target dose between the origin and enhancement boundary, with 5% of the maximum dose fixed 15 mm beyond the enhancement boundary with margin, which determines the gradient of the dose boundary. To maintain a realistic, non-zero dose throughout the brain, we fix the dose to be zero only at the far boundary of the one dimensional domain. These points are then interpolated with a spline interpolation algorithm, guaranteeing the smoothness and differentiability of the dose function  $d(x, t)$ .

### 3.6 Radiation dose fractionation

Clinically, radiation dose is delivered with the intent of maximizing (tumor) effect while at the same time minimizing (normal tissue) toxicity. This often leads to daily dosages of between 1 and 2.5 Gy. Hyper- and hypo-fractionation of the standard dose involve decreasing the incremental dose amount with an increase in frequency or vice versa, respectively [41,42]. Although thresholds for radiation toxicity and radiation-induced necrosis exist in clinical practice [43], we investigate the effects of accelerated

**Fig. 2** **a** Two-dimensional cross section of actual dose distribution for a patient with a GBM. Enhancement margin is nonuniform in order to avoid high doses of radiation to the brain stem. **b** One-dimensional dose distribution created with a spline interpolation of nine reference points. **c** Cumulative dose distribution showing enhancement region plus margin for initial and boost phases of dose delivery for the standard treatment scheme



or decelerated treatment on a virtual tumor, ignoring the thresholds of toxicity. This assumption is not grossly negligent, as current treatment practices such as gamma-knife [44] deliver a whole course (>50 Gy) of radiation treatment in a single dose with

the conscious trade off of cell kill for tangential toxicity-albeit the dose distribution for gamma-knife is tailored much more closely to the enhancing region with a 50% decrease in dose magnitude over 2 mm typically attained, unlike the above, for which a 50% decrease in dose magnitude spans as much as 10 mm.

## 4 Results

We simulate the growth and treatment of a virtual tumor under a variety of treatment schedules and dose distributions as well as investigate the differences in response using different metrics. We characterize the virtual tumor with parameter values as follows:  $D = 1.43 \text{ cm}^2/\text{year}$ ,  $\rho = 16.25 /\text{year}$ , which serve as representative means of published ranges [2].

### 4.1 Estimating radiation sensitivity

The National Cancer Institute determines tumor response to treatment using the Response Evaluation Criteria in Solid Tumors (RECIST) [45] as follows: disappearance of all target lesions, complete response (CR), 30% decrease in pre-treatment diameter, partial response (PR), 20% increase in pre-treatment diameter progressive disease (PD) and small changes that do not meet the above criteria stable disease (SD). The symmetry of our simulations allow us to consider the RECIST criteria in the context of radial progression of the tumor rather than diameter. Due to their significant resistance to radiotherapy and aggressive growth, glioma radiation response is generally classified as PD to PR, with response measured on T1Gd; accordingly, we define the typical response window (TRW) as 30% decrease to 20% increase in pre-treatment radius immediately after therapy. Given this rather coarse but nevertheless contemporary and pragmatic view of treatment response, we can establish a realistic range for our radiation sensitivity parameter,  $\alpha$ , for the virtual tumor. Using an iterative approach with a fixed incremental change in  $\alpha$ , we simulated a standard course of XRT on the virtual tumor for a large set of  $\alpha$  values. The TRW restricts the range of reasonable radiation sensitivities to  $0.025 \text{ Gy}^{-1} \leq \alpha \leq 0.033 \text{ Gy}^{-1}$ , well within published ranges calculated for gliomas [37,46] (Fig. 3). Although the figure may suggest a linear relationship between  $\alpha$  and T1Gd radius at the end of therapy, additional simulations reveal a highly non-linear pattern for changes in  $\alpha$ ,  $D$  or  $\rho$ .

The following simulations were performed with  $\alpha = 0.0305 \text{ Gy}^{-1}$ , resulting in ~25% decrease in pre-treatment radius for the standard XRT schedule, an optimistic and above average response to treatment.

### 4.2 Treatment schedule and fractionation

Several dose fractionation schemes were simulated based on the number of fractions per day (FPD) and total DOT in intervals of 1–4 FPD and 1, 5, 10, 15, 40 DOT (Table 1) and 1, 5, 15–45 DOT (Fig. 4), respectively [41,42,47,48]. The maximum regional total dose was held constant at 61.2 Gy, with per fraction dose distributions

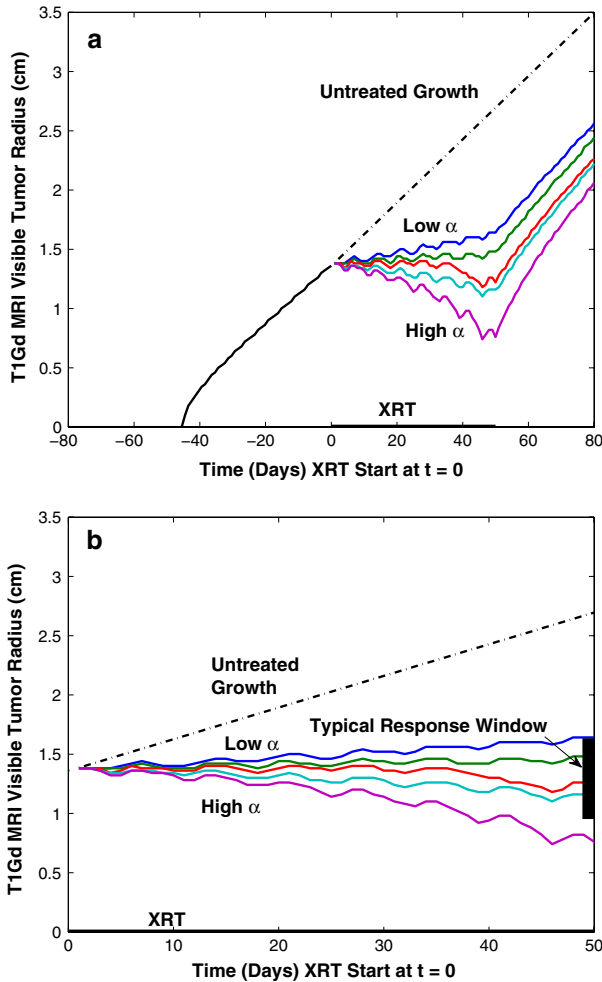


**Fig. 3** a Simulated tumor growth and response prior to, during and after XRT as measured on T1Gd. *Solid black line* shows no visible tumor for ~30 days. Time  $t = 0$  days corresponds to the beginning of standard XRT simulated with range of sensitivity values  $0.025 \text{ Gy}^{-1} \leq \alpha \leq 0.036 \text{ Gy}^{-1}$ . *Dotted black line* shows projected untreated tumor growth using Fisher's approximation:  $D = 1.43 \text{ mm}^2/\text{year}$ ,  $\rho = 16.52 \text{ /year}$ . **b** Detail of **a** with typical response window (TRW) of  $-30$  to  $+20\%$  of pre-treatment radius

determined according to the standard treatment protocol such that the sum of all dose fractions did not exceed  $61.2 \text{ Gy} + 5\%$ . For XRT schedules with DOT less than 10 days, the BT was set to one day and dose distributions computed consistent with the standard treatment course.

A clear benefit of a mathematical simulation of radiation therapy is the ability to observe tumor response at any time during the course of treatment. This of course is not the case with real tumors, and the relative infrequency of MRI observations suggests we consider a clinically based response metric relative to the last observation point, usually at the beginning of therapy. MRI observations to measure response to therapy

**Table 1** Forty treatment schedules were simulated: 1–4 FPD and 1, 5, 10, 15, . . . , 40 DOT

XRT fractionation array responses: percent effect

	T1Gd				T2			
	1FPD	2FPD	3FPD	4FPD	1FPD	2FPD	3FPD	4FPD
Mean	57.0	-6.8	-27.3	-36.7	14.3	-14.4	-21.8	-25.3
Median	90.6	-15.2	-32.6	-40.6	13.7	-14.6	-22.6	-25.9
Maximum	<b>100</b>	100	71.0	49.3	<b>72.6</b>	26.4	22.6	17.9

Response to each was measured as percent change in pre- to post-treatment radius as in (12), with 100 indicating a CR, 0 no response and negative values indicating tumor progression. Mean, median and maximum values of percent effect were computed over all DOT for each FPD. Clearly 1 FPD will suffice to yield the best result on both T1Gd and T2 (*bold*)

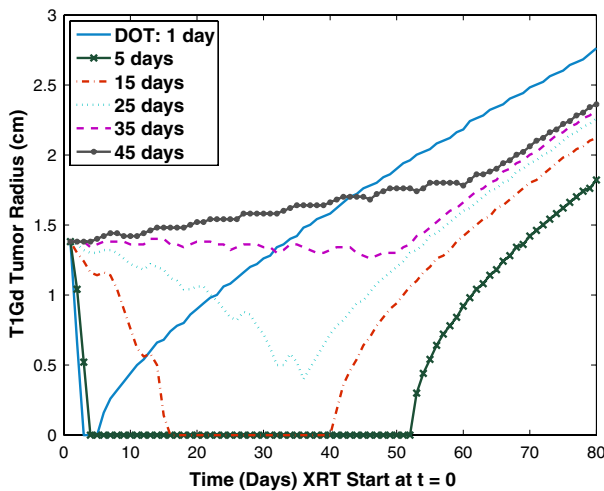


**Fig. 4** Simulated tumor response to XRT using a one per day dose delivery scheme for several days of therapy with the total dose held constant at 61.2 Gy

are usually conducted within a week after the treatment is completed although MRI’s may be conducted at any time during therapy. For simplicity, we will assume that the earliest potential MRI observation is immediately after the last treatment. Therefore, response to therapy was measured relative to the tumor size at the start of therapy by taking the percent reduction of pre- versus post-treatment radii for T1Gd and T2 each, as follows:

$$\text{percent effect} = \frac{(r_{\text{start}} - r_{\text{end}})}{r_{\text{start}}} \tag{11}$$

where  $r_{\text{start}}$  = radius at start of XRT and  $r_{\text{end}}$  = radius at end of XRT for each T1Gd and T2 measures. Therefore a CR, or a complete disappearance of tumor results in 100% effect, no response results in 0% effect, and negative effect implies tumor progression. Clearly for the dose distributions considered here, we have  $\lim_{d(x,t) \rightarrow 0} (1 - S) = 0$

**Table 2** Forty treatment schedules were simulated using two different dose distribution techniques: 1–4 FPD and 1, 5, 10, 15, . . . , 40 DOT, equal fractions and boost, respectively

XRT dose distribution responses:

$$\text{Net effect} = \text{percent effect}_{\text{equal fractions}} - \text{percent effect}_{\text{boost}}$$

	T1Gd				T2			
	1FPD	2FPD	3FPD	4FPD	1FPD	2FPD	3FPD	4FPD
Mean	0.1	0.1	-0.1	0.1	0.4	-0.4	-0.3	-0.4
Median	0	0	0	0	0	-0.5	0	0
Maximum	13.0	2.9	2.9	1.5	3.8	0.9	0	0
Minimum	-10.1	-1.5	-2.9	-1.5	-1.9	-0.9	-0.9	-0.9

Net effect quantifies the difference in effect between responses and the dose distribution techniques for each treatment. Mean, median, maximum and minimum values were computed over all DOT for each FPD. The widest range of values comes from the 1 FPD regimen, although comparisons across mean and medians suggest very little difference between boost and equal fractions efficacy in general

for any fixed  $x$  and  $t$ , so we expect the response to hyper-fractionation to go to zero as the number of fractions increase, leading to decreased response per fraction and therefore a decrease in overall response. Conversely, as dose increases,  $(1 - S) \rightarrow 1$ , we expect a large per fraction response and, therefore, an increase in overall response. Figure 4 reveals a wide range of responses even within the conventional single dose per day regimen, with 12.2 Gy daily for 5 days giving the best result in this simulation, and results of simulations involving all 40 treatment schedules confirm the expectation in general (Table 1).

Investigation of treatment response to schedules in the array reveals a dramatically increased response on T1Gd for treatment schedules involving 1 FPD (Tables 1, 2), compared to 2, 3 or 4 FPD. T2 showed much less response across all schedules than T1Gd, by at least 40%, consistent with the dose decreasing radially from the T1Gd abnormality for a typical dose at the T2 radius + 20 mm. The 5 DOT, 1 FPD regimen yielded the best response of 100 and 72% reduction in tumor radius on T1Gd and T2 (Table 1), respectively. Only 11 of the 40 treatment schedules yielded responses within the TRW which included the standard therapy. The single fraction per day treatment provided the best response on both T1Gd and T2 by at least 23% compared to the other fractionations, excluding the near equivalence of all fractionations for treatment delivered on a single day, which borders on fatal radiation toxicity [3].

### 4.3 Radiation dose delivery

Additionally, for each treatment schedule discussed above, simulations were conducted using dose distributions determined in each of two ways: equal fractions per treatment, and adjusted fractions based on the standard BT and BR as follows:

- Equal Fractions: a single dose distribution is formed as a sum of initial and boost phase distributions as determined by the pre-treatment tumor concentration, divided by two, such that the total dose distribution is the product of DOT and FPD and the per fraction dose distribution not to exceed 61.2 Gy + 5%. The BR is

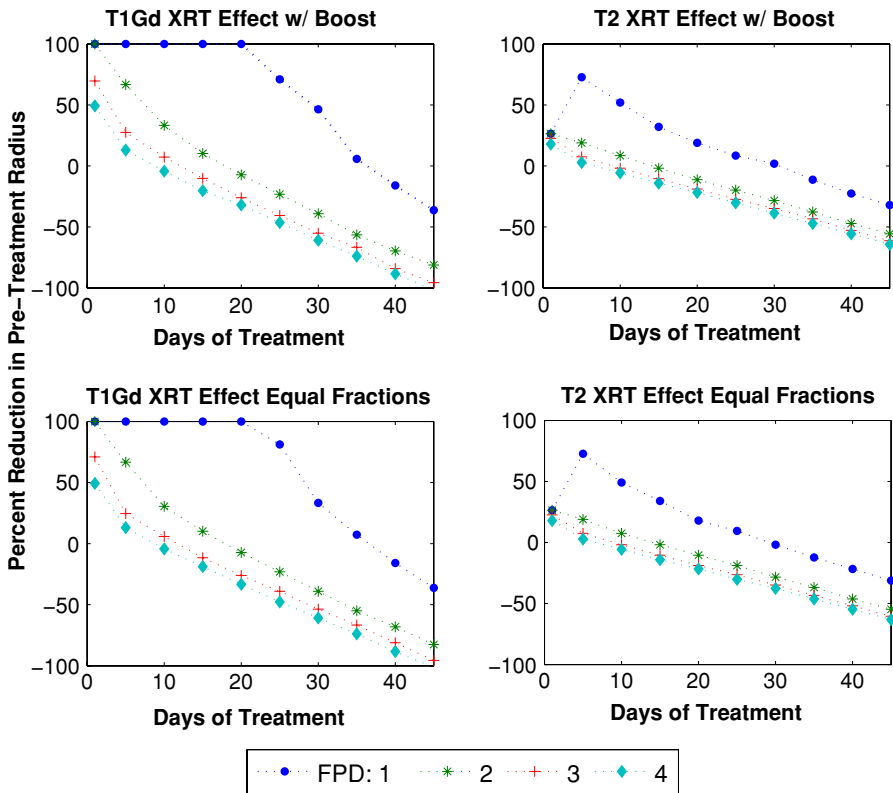


**Fig. 5** Response to therapy as measured by percent reduction in pre-treatment radius at the end of therapy as visible on T1Gd and T2 MRI for 1, 5, 10, 15, . . . , 40DOT at each of 1–4 dose fractions per day using two different dose distribution schemes: equal fractions and boost. Total dose held constant at 61.2 Gy

determined prior to therapy instead of at the beginning of the BT, and is incorporated into the per fraction dose distribution which does not change shape or geometry at all during treatment.

- Boost: for XRT schedules with DOT less than 10 days, the BT was set to one day and dose distributions are computed consistent with the standard treatment course. For schedules involving 15 or more DOT, the boost time and BR were determined at the 6th day before the end of therapy, with the total dose distribution not to exceed 61.2 Gy + 5%.

Figure 5 illustrates no qualitative difference between dose distribution schemes. This is significant and surprising in light of the specificity with which the boost dose distribution targets the T2 region for the majority of treatment. Quantitative differences between the two dose distribution schemes were taken to be the difference in percent effect as

$$\text{net effect} = \text{percent effect}_{\text{equal fractions}} - \text{percent effect}_{\text{boost}} \tag{12}$$

across all treatment schedules.

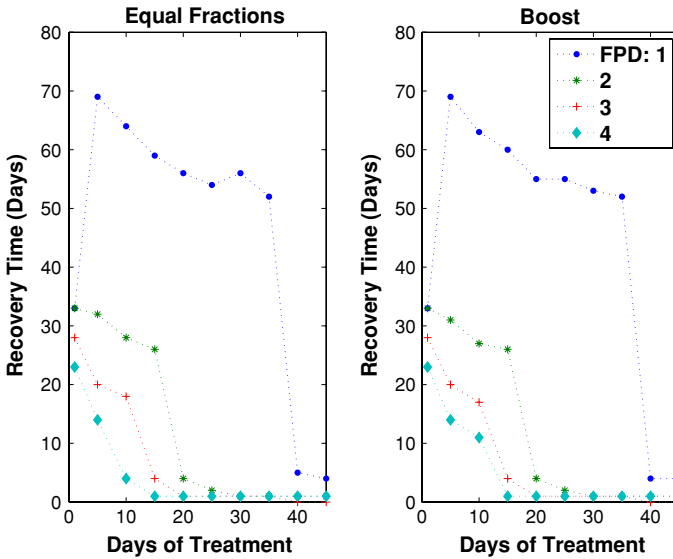


**Fig. 6** Recovery time, measured as the minimum time for which the tumor attains its pre-treatment radius for each of four fractions per day and 1, 5, 10, 15, . . . , 40DOT. Recovery time was set to one day for treatments that yielded no response

The net effect was between  $\pm 5\%$  for all but two cases. The largest net effects in magnitude equaled 13 and  $-10\%$  for the 1 FPD regimen at 30 and 25 DOT, respectively, as measured on T1Gd. As shown in Table 2, the mean net effect for T1Gd favored equal fractions for 3 out of 4 fractionation schemes, however, 3 out of the 4 schemes for T2 favor boost. The median net effect is zero for all but 2 FPD on T2. This suggests that the differences between the dose distributions are negligible for a large majority of the treatment schedules simulated.

#### 4.4 Recovery time

We define recovery time (RT) to be the minimum amount of time between the start of therapy and the time at which the tumor re-attains its pre-treatment radius as measured on T1Gd. For treatments which yield no response, the recovery time is defined as one day.

Recovery time was measured for all 40 treatment schedules and for both dose distribution schemes. The recovery time falls outside of the DIT and thus a clinically observable response for only 42% of the total simulated treatment schedules and fractionations in the array, including the standard treatment. Therefore in 58% of the cases, the benefit of therapy was either not clinically observable or was not beneficial at any point.

Interestingly, Fig. 6 reveals a sharp decrease in recovery time from the standard treatment and the next DOT increment, suggesting that, although not optimal, the conventional course of therapy does avoid a drastic reduction in efficacy by only a few tenths of a Gy in dose per treatment. Additionally, the difference in recovery time for

equal fractions versus boost dose distributions have a mean and median of zero, with max increase of 7 days for the least effective fractionation, 4 FPD at 10 DOT.

The recovery time analysis suggests that conventional high dose hypo-fractionation therapy, similar to gamma-knife procedures, yields the highest recovery time and, therefore, delays progression of the tumor the most. Moreover, the conventional, daily fractionation is vastly more effective at prolonging recovery time than multiple fractions per day.

## 5 Discussion

Although highly idealized, this simple extension of Swanson's fundamental model for glioma growth and invasion [4] sheds light on the potential to incorporate existing quantifications of radiation efficacy, medical and radiological imaging into in vivo tumor modeling. Investigations into fractionation schedules, dose distribution and radiation sensitivity ranges reveal the highly individualized nature of dose delivery and non-linear response to radiation therapy. The results suggest that the conventional course of treatment, involving radiation dose administered on a per day basis, is much more effective than several treatments per day, and that an optimal response is produced by a low frequency, high dose scheme similar to radio-surgical procedures like gamma-knife. Simulated responses to conventional treatment mirror responses expected for gliomas within published ranges, and suggest that the model and radiation sensitivity parameter  $\alpha$  qualitatively reflect this phenomenon.

Results of simulations of the XRT schedule and fractionation array show surprisingly little difference between the boost and equal fraction dose distributions, particularly with respect to T2 response. This is surprising because of the specificity with which the XRT dose distribution targets the T2 region during the initial phase of conventional XRT treatment. This suggests that the BT and BR have little net effect on either the T1Gd or T2 visible portions of the tumor, consistent with recurrence patterns and the invasive, treatment-resistant nature of gliomas. Although the T1Gd abnormality only indirectly represents the bulk tumor mass through its leaky neovasculature and may not shrink to reflect the instantaneous effect of XRT on the tumor, we have used it as representative of the concentration of viable cells in that area, to remain consistent with Swanson's previous work [2].

A significant advantage of our model over others [15,48–50] is the relatively small number of parameters and input data necessary to run the model ( $D$ ,  $\rho$  and 2 pre-treatment MRIs). Our ability to calculate simulation parameters based solely on clinical observations yields a highly individualized and clinically relevant model which is able to capture macroscopic tumor characteristics and which does not ignorantly simplify or overcomplicate the mechanisms modeled. Although other models [15,48–50] attempt a more complicated and mechanistic approach to modeling XRT and response, none of them can be tailored to an individual via the only clinically available metric for monitoring disease progression, namely MRI and PET imaging.

Avenues for further investigation include higher dimensional simulations without the assumption of spherical symmetry, inclusion of chemo and resection therapies, quantification and minimization of radiation toxicity, incorporation of cell cycle dynamics as they relate to increased radiation susceptibility, and development of a

more representative measure of the number of glioma cells remaining after XRT, as well as the incorporation of PET imaging to identify molecular level resistance mechanisms such as hypoxia.

**Acknowledgments** The authors gratefully acknowledge the support of the McDonnell Foundation, the Shaw Professorship and the Academic Pathology Fund.

## References

1. Alvord EC Jr, Shaw CM (1991) Neoplasms affecting the nervous system in the elderly. In: Duckett S (ed) *The pathology of the aging human nervous system*. Lea & Febiger, Philadelphia, pp 210–281
2. Harpold HL, Alvord EC Jr, Swanson KR (2007) The evolution of mathematical modeling of glioma proliferation and invasion. *J Neuropathol Exp Neurol* 66:1–9
3. Hall E (1994) *Radiobiology for the radiologist*. Lippincott, Philadelphia, pp 478–480
4. Swanson KR, Rockne R, Rockhill JK, Alvord EC Jr (2007) Mathematical modeling of radiotherapy in individual glioma patients: quantifying and predicting response to radiation therapy. In: *AACR annual meeting*, Los Angeles
5. Alvord EC Jr (1995) Patterns of growth of gliomas. *Am J Neuroradiol* 16:1013–1017
6. Nelson SJ, Cha S (2003) Imaging glioblastoma multiforme. *J Cancer* 9:134–145
7. Bloor R, Templeton AW, Quick RS (1962) Radiation therapy in the treatment of intracranial tumors. *Am J Roentgenol Radium Ther Nucl Med* 87:463–472
8. Chicoine M, Silbergeld D (1995) Assessment of brain tumour cell motility in vivo and in vitro. *J Neurosurg* 82:615–622
9. Swanson KR (1999) *Mathematical modeling of the growth and control of tumors*, PhD Thesis, University of Washington
10. Woodward DE, Cook J, Tracqui P, Cruywagen GC, Murray JD, Alvord EC Jr (1996) A mathematical model of glioma growth: the effect of extent of surgical resection. *Cell Prolif* 29:269–288
11. Tracqui P, Cruywagen GC, Woodward DE, Bartoo GT, Murray JD, Alvord EC Jr (1995) A mathematical model of glioma growth: the effect of chemotherapy on spatio-temporal growth. *Cell Prolif* 28:17–31
12. Murray JD (2002) *Mathematical biology I. An introduction*, 3rd edn. Springer, New York, pp 437–460
13. Carlone M, Wilkins D, Raaphorst P (2005) The modified linear-quadratic model of Guerrero and Li can be derived from a mechanistic basis and exhibits linear-quadratic-linear behaviour. *Phys Med Biol* 50:L9–L13 (author reply L13–L15)
14. Sachs RK, Hlatky LR, Hahnfeldt P (2001) Simple ODE models of tumor growth and anti-angiogenic or radiation treatment. *Math Comp Model* 33:1297–1305
15. Cunnings JR, Niederer J (1972) Mathematical-model for cellular response to radiation. *Phys Med Biol* 17:685
16. Jones B, Dale RG (1995) Cell loss factors and the linear-quadratic model. *Radiother Oncol* 37:136–139
17. Taylor H, Karlin S (1984) *An introduction to stochastic modeling*. Academic Press, Chestnut Hill
18. Swanson KR, Alvord EC Jr, Murray JD (2000) A quantitative model for differential motility of gliomas in grey and white matter. *Cell Prolif* 33:317–329
19. Burgess PK, Kulesa PM, Murray JD, Alvord EC Jr (1997) The interaction of growth rates and diffusion coefficients in a three-dimensional mathematical model of gliomas. *J Neuropathol Exp Neurol* 56:704–713
20. Swanson KR, Alvord EC Jr (2002) The concept of gliomas as a “traveling wave”: the application of a mathematical model to high- and low-grade gliomas. *Can J Neurol Sci* 29:395
21. Alvord EC Jr (1991) Simple model of recurrent gliomas. *J Neurosurg* 75:337–338
22. Guenther R, Lee J (1988) *Partial differential equations of mathematical physics and integral equations*. Prentice Hall, Englewood Cliffs, pp 144–187
23. Swanson KR, Alvord EC Jr, Murray JD (2002) Virtual brain tumours (gliomas) enhance the reality of medical imaging and highlight inadequacies of current therapy. *Brit J Cancer* 86:14–18
24. Capelle L, Mandonnet E, Broet P, Swanson KR, Carpentier A, Duffau H, Delattre JY (2002) Linear growth of mean tumor diameter in WHO grade II gliomas. *Neurology* 58:A13
25. Swanson KR, Alvord EC Jr (2002) A biomathematical and pathological analysis of an untreated glioblastoma. In: *International congress on neuropathology*, Helsinki

26. Mandonnet E, Delattre JY, Tanguy ML, Swanson KR, Carpentier AF, Duffau H, Cornu P, Van Effenterre R, Alvord EC Jr, Capelle L (2003) Continuous growth of mean tumor diameter in a subset of grade II gliomas. *Ann Neurol* 53:524–528
27. Mandonnet E, Broët P, Swanson KR, Carpentier AF, Delattre JY, Capelle L (2002) Linear growth of mean tumor diameter in low grade gliomas. *Neurology* 58(Suppl 13):A13
28. Swanson KR, Rostomily RC, Alvord EC Jr (2003) Confirmation of a theoretical model describing the relative contributions of net growth and dispersal in individual infiltrating gliomas. *Can J Neurol Sci* 30:407–434
29. Swanson KR, Alvord EC Jr (2001) A 3D quantitative model for brain tumor growth and invasion: correlation between the model and clinical behavior. *Neuro Oncol* 3:323
30. Swanson KR, Alvord EC Jr, Murray JD (2003) Virtual resection of gliomas: effects of location and extent of resection on recurrence. *Math Comp Model* 37:1177–1190
31. Tilly N, Brahme A, Carlsson J, Glimelius B (1999) Comparison of cell survival models for mixed LET radiation. *Int J Radiat Biol* 75:233–243
32. Sachs RK, Hahnfeldt P, Brenner DJ (1997) The link between low-LET dose-response relations and the underlying kinetics of damage production/repair/misrepair. *Int J Radiat Biol* 72:351–374
33. Wheldon TE, O'Donoghue JA (1990) The radiobiology of targeted radiotherapy. *Int J Radiat Biol* 58:1–21
34. Enderling H, Anderson AR, Chaplain MA, Munro AJ, Vaidya JS (2006) Mathematical modelling of radiotherapy strategies for early breast cancer. *J Theor Biol* 241:158–171
35. Jones B, Dale RG (1999) Mathematical models of tumour and normal tissue response. *Acta Oncol* 38:883–893
36. Lee SP, Leu MY, Smathers JB, McBride WH, Parker RG, Withers HR (1995) Biologically effective dose distribution based on the linear quadratic model and its clinical relevance. *Int J Rad Oncol Biol Phys* 33:375–389
37. Garcia LM, Leblanc J, Wilkins D, Raaphorst GP (2006) Fitting the linear-quadratic model to detailed data sets for different dose ranges. *Phys Med Biol* 51:2813–2823
38. McAneny H, O'Rourke SF (2007) Investigation of various growth mechanisms of solid tumour growth within the linear-quadratic model for radiotherapy. *Phys Med Biol* 52:1039–1054
39. Skeel R, Berzins M (1990) A method for the spatial discretization of parabolic equations in one space variable. *SIAM J Sci Stat Comput* 11:1–32
40. Hendry JH, Bentzen SM, Dale RG, Fowler JF, Wheldon TE, Jones B, Munro AJ, Slevin NJ, Robertson AG (1996) A modelled comparison of the effects of using different ways to compensate for missed treatment days in radiotherapy. *Clin Oncol (R Coll Radiol)* 8:297–307
41. O'Donoghue JA (1997) The response of tumours with gompertzian growth characteristics to fractionated radiotherapy. *Int J Radiat Biol* 72:325–339
42. Wheldon TE, Berry I, O'Donoghue JA, Gregor A, Hann IM, Livingstone A, Russell J, Wilson L (1987) The effect on human neuroblastoma spheroids of fractionated radiation regimes calculated to be equivalent for damage to late responding normal tissues. *Eur J Cancer Clin Oncol* 23:855–860
43. Abou-Jaoude W, Dale R (2004) A theoretical radiobiological assessment of the influence of radionuclide half-life on tumor response in targeted radiotherapy when a constant kidney toxicity is maintained. *Cancer Biother Radiopharm* 19:308–321
44. Gerosa M, Nicolato A, Foroni R (2003) The role of gamma knife radiosurgery in the treatment of primary and metastatic brain tumors. *Curr Opin Oncol* 15:188–196
45. Padhani AR, Ollivier L (2001) The RECIST (response evaluation criteria in solid tumors) criteria: implications for diagnostic radiologists. *Br J Radiol* 74:983–986
46. Qi XS, Schultz CJ, Li XA (2006) An estimation of radiobiologic parameters from clinical outcomes for radiation treatment planning of brain tumor. *Int J Radiat Oncol Biol Phys* 64:1570–1580
47. Wheldon TE, Deehan C, Wheldon EG, Barrett A (1998) The linear-quadratic transformation of dose-volume histograms in fractionated radiotherapy. *Radiother Oncol* 46:285–295
48. Ribba B, Colin T, Schnell S (2006) A multiscale mathematical model of cancer, and its use in analyzing irradiation therapies. *Theor Biol Med Model* 3
49. Stamatakis GS, Antipas VP, Uzunoglu NK, Dale RG (2006) A four-dimensional computer simulation model of the in vivo response to radiotherapy of glioblastoma multiforme: studies on the effect of clonogenic cell density. *Br J Radiol* 79:389–400
50. Enderling H, Chaplain MA, Anderson AR, Vaidya JS (2007) A mathematical model of breast cancer development, local treatment and recurrence. *J Theor Biol* 246:245–259